Sensing and Bio-Sensing Research 48 (2025) 100790

Contents lists available at ScienceDirect

Sensing and Bio-Sensing Research

journal homepage: www.elsevier.com/locate/sbsr

Adaptive resolution in speckle displacement measurement using optimized grid-based phase correlation and statistical refinement

Hamed Sabahno [a], Satyam Paul [b], Davood Khodadad [a,*]

[a] Department of Applied Physics and Electronics, Umeå University, 90187 Umeå, Sweden
[b] Division of Product Realisation, School of Innovation, Design and Engineering, Mälardalens University, 63217 Eskilstuna, Sweden

ARTICLE INFO

Keywords:
Deformation measurement
Speckle metrology
Quality control
Non-destructive testing (NDT)
Phase correlation
Adaptive resolution
Material surface characterization

ABSTRACT

Speckle metrology is a powerful optical sensing tool for non-destructive testing (NDT) and advanced surface characterization, enabling ultra-precise measurements of surface deformations and displacements. These capabilities are critical for material analysis and surface assessment in sensing-driven applications. However, traditional correlation methods often struggle to balance resolution and robustness, particularly when simultaneously measuring both small- and large-scale deformations in noisy, high-frequency data environments. In this paper, we present an adaptive resolution approach for speckle displacement measurement that combines grid-based phase correlation with statistical refinement for enhanced accuracy and resolution.

Unlike traditional phase correlation techniques that rely on global correlation, our method introduces a flexible grid-based framework with localized correlation and dynamic overlap adjustments. To improve measurement performance, we developed an optimization technique that uses the median absolute deviation of residuals between reference and deformed images, enabling the algorithm to automatically adapt grid sizes based on local deformation characteristics. This allows it to handle both small- and large-scale deformations simultaneously and effectively. The approach resulted in a relative error reduction of up to 14 % compared to the best of the results obtained using a manually fixed grid size.

The proposed sensing methodology is validated through a series of numerical simulations and experimental studies, including controlled deformations with a micrometer translation stage and random speckle displacements on water-sprayed surfaces. Results demonstrate that our method can accurately detect both known and unknown deformations with high accuracy and precision, outperforming traditional techniques in terms of adaptability and robustness, particularly for surface deformation analysis.

1. Introduction

Optical metrology and non-destructive evaluation (NDE) are fundamental in engineering, where accurate and real-time sensing and measurement of parameters like deformation, roughness, shape, refractive index, and temperature are crucial for assessing material integrity and performance [1–6]. Advanced optical techniques such as interferometry, spectroscopy, and laser-based imaging, provide the high-resolution, non-contact capabilities essential for these measurements and are indispensable in a wide range of engineering applications. Among these methods, speckle metrology has emerged as a highly adaptable and precise approach, enabling detailed measurement of surface deformations, structural displacements, and shape measurements [7–11]. These capabilities make speckle metrology a versatile tool, suited not only for quality control and structural monitoring but also for experimental investigations in dynamic and challenging environments, where optical techniques drive innovation in metrological accuracy and adaptability for engineering solutions [12–14].

Speckle patterns form when coherent light, such as laser light, scatters off rough or irregular surfaces, producing an interference pattern with unique intensity distributions [7]. By analyzing shifts in these patterns, speckle metrology provides exceptional sensitivity to micro-scale surface deformations, making it highly valuable optical sensing technique in applications requiring precise surface measurements. The technique's ability to detect minute variations in surface texture, deformation, and strain makes it a cornerstone for modern non-destructive evaluation and material characterization [14]. Furthermore, recent advances in digital speckle interferometry and computational

* Corresponding author.
E-mail address: davood.khodadad@umu.se (D. Khodadad).

https://doi.org/10.1016/j.sbsr.2025.100790
Received 1 January 2025; Received in revised form 11 April 2025; Accepted 14 April 2025
Available online 15 April 2025

methods have expanded its applicability, enabling real-time, high-resolution measurements for both micro- and macro-scale surface changes [15–19].

Speckle displacement analysis, a key aspect of speckle metrology, involves tracking the spatial shifts (displacements) in speckle patterns caused by deformations or surface changes [7,20]. These displacements can manifest in various forms, translation, rotation, deformation, shear, or changes in surface texture; and each type of displacement alters the speckle pattern uniquely. Accurately interpreting these displacements provides crucial insights into surface behavior, making speckle analysis a powerful sensing tool for real-time surface monitoring across diverse fields such as material science, optics, fluid mechanics, medical imaging and diagnostics, agriculture and more [12,21–25].

Traditionally, methods like optical flow, template matching, and feature-based tracking have been employed for displacement analysis. However, these techniques often struggle in the context of speckle images due to their high-frequency content and noisy nature. Optical flow methods, for example typically rely on smoothing techniques to reduce noise, which inadvertently removes high-frequency information and minute displacements [26]. As a result, optical flow is often less effective when dealing with fine movements or high-frequency patterns, such as those seen in speckle and material surface images. Feature-based methods are also limited by the lack of distinct features in speckle images [27–29]. In contrast, correlation-based algorithms are highly effective for displacement measurement in speckle patterns [21,25,30,31]. Unlike methods that rely on feature extraction or intensity changes, correlation-based algorithms measure the statistical similarity between regions of the speckle pattern before and after displacement. The high contrast and random structure of speckle patterns make them particularly suitable for correlation-based approaches, which can accurately detect minute displacements without relying on identifiable features. This makes them ideal for handling high-frequency and noisy data that would typically hinder other methods [32].

Digital Image Correlation (DIC) algorithms can be categorized into two main types: intensity correlation and phase correlation. Beyond the input type, the computation of correlation can happen either locally or globally [33]. In local correlation, the image is divided into smaller grids (subimages), and displacement and deformations are tracked within each subset individually [34]. This localized approach allows for higher accuracy in detecting small, localized deformations, but it may introduce inconsistencies at the boundaries between subsets. On the other hand, global correlation [35,36] considers the entire image, providing consistent displacement measurement across the entire field but potentially lowering the resolution and missing minute deformations.

The accuracy of correlation-based methods is influenced by the correlation criteria and the size of the grid or subsets used in local computation [25]. Global computations tend to smooth out small-scale movements, making it harder to track subtle local small shifts. In contrast, local computations can capture fine details, but the boundaries between subsets require careful handling (interpolation) to ensure displacement continuity [33].

Among correlation-based techniques, Phase Correlation (PC) [37] is particularly notable for its computational efficiency and robustness in the frequency domain, achieved through the Fast Fourier Transform (FFT). When applied to speckle metrology, PC offers distinct advantages over intensity-based methods, which depend on image intensity and content. Instead, PC focuses on phase information, making it less sensitive to variations in contrast and brightness. This phase-based sensing approach ensures that PC is invariant to global linear changes in illumination, resulting in sharper and more precise correlation peaks. Moreover, because phase differences across all frequencies contribute equally, PC is highly resistant to frequency-dependent noise and localized disruptions, ensuring that the dominant phase difference and thus the correlation peak remains stable. This robustness extends to handling significant intensity variations and dynamic changes in illumination, making PC particularly suitable for noisy, high-frequency data like speckle patterns. Its ability to maintain stability under varying lighting conditions makes it an ideal technique for surface analysis, where illumination or contrast fluctuations are common challenges [36].

While conventional PC typically employs global correlation, where the entire image is analyzed as a whole, we propose a novel hybrid approach that integrates local correlation into PC, enhancing traditional methods through adaptive resolution in speckle displacement measurement. In traditional sensing approaches, which rely on fixed grid sizes, there is often a trade-off between detecting small- and large-scale deformations. Smaller grids can capture fine details but risk missing larger displacements, while larger grids are better suited for detecting broader deformations but lack the resolution needed for precise detection of smaller-scale changes.

Our method addresses these limitations by incorporating a grid-based framework with dynamic overlap adjustments and optimization via statistical refinement. By dynamically adjusting grid sizes, we achieve adaptive resolution for displacement detection. This adaptive resolution ensures that both small- and large-scale deformations are accurately detected without the need to compromise between resolution and coverage. By automatically refining grid sizes based on the deformation characteristics in different regions, our approach significantly improves resolution and adaptability across diverse surface conditions. This combination of local correlation, PC, and dynamic grid adjustments enables accurate and precise detection of both subtle and significant surface deformations.

In this paper, we present both numerical simulations and experimental validation of the proposed method. The experimental validation includes two types of deformation scenarios: controlled deformation and uncontrolled deformation. In the controlled deformation case, we apply the proposed method to detect speckle displacements over time between consecutive images captured after known speckle translations using a micrometer translation stage. For the uncontrolled deformation, we apply the method to detect speckle displacements caused by unknown surface deformation, created by spraying water on a cardboard surface. These experiments demonstrate the method's ability to track both known and unknown surface displacements with high accuracy and precision, outperforming traditional correlation techniques in adaptability and robustness.

This paper is structured as follows: In Section 1, we discuss the significance of speckle metrology in deformation analysis through speckle displacement measurements. We review well-established displacement measurement methods and highlight the limitations that our contribution aims to address. Section 2 details the proposed adaptive resolution grid-based phase correlation algorithm, including its theoretical foundations, the integration of dynamic overlap, and the effective grid size mechanism, which allow for robust detection of both small and large displacements. Section 3 presents a simulation study in which the method is applied to simulated cases to evaluate its performance. We introduce an optimization technique based on median absolute deviation (MAD) [38,39] to dynamically adjust the effective grid size and enhance the accuracy of displacement measurement in varying deformation conditions. Section 4 describes the experimental setup and validation process, where the proposed algorithm is tested against both controlled and uncontrolled surface deformations, including real-world applications such as micrometer-induced displacements and random speckle movements caused by water spray. The results confirm the method's robustness, adaptability, and accuracy in real-world scenarios. Section 5 discusses the significance of the findings in greater detail, emphasizing the advantages of our adaptive approach over traditional methods. This section also outlines potential improvements, including the extension of the algorithm to detect additional types of deformations, such as local rotations, and the exploration of non-symmetrical grid size adjustments. Finally, we offer concluding remarks on the method's broader applicability and suggestions for future research directions.

2. Theory and method

In this section, we present the methodological framework and theoretical principles that guide our approach to speckle displacement measurement. The proposed method, based on adaptive resolution grid-based phase correlation, allows for precise detection of displacements in speckle patterns by dividing the image into grids and dynamically adjusting the overlap between grids. By optimizing the overlap using MAD, the algorithm is capable of detecting both small, fine-scale displacements and larger displacements that occur across the image. This adaptability ensures that the method remains robust, even in challenging conditions such as the presence of outliers or varying displacement scales in terms of size and area. The following subsections provide an explanation of the proposed algorithm's operational steps and the mathematical foundations underlying image registration and displacement estimation. This includes the theoretical framework for accurately aligning images and calculating displacement vectors, ensuring accuracy in the detection of deformations.

2.1. The algorithm

The following algorithm outlines the steps of the proposed adaptive resolution grid-based phase correlation method for detecting and measuring speckle displacements:

Algorithm 1
Adaptive Resolution Grid-Based Phase Correlation for Speckle Displacement Measurement.

Input:
- Two images: reference image I_{ref}, deformed image I_{def}
- Grid size: S (initially small for high resolution)
- Overlap: $O_{start} \rightarrow O_{end}$ (changes effective grid size)

Output:
- Displacement map: $\boldsymbol{A}$

1: Load images I_{ref} and I_{def}
Initialize the reference and deformed images

2: Define grids of size S for both I_{ref} and I_{def}
Divide the images into sub-images (grids) based on the defined size

3: For each grid **do**
Iterate over each grid in the X and Y directions

4: For each overlap $O \in [O_{start}, O_{end}]$ **do**
Iterate over each overlap

5: Perform phase correlation to compute displacement for the grid
Detect displacements between the grids in I_{ref} and I_{def}

6: Translate the deformed grid to the origin using detected displacement
Align the deformed image to the reference based on the detected displacement

7: Calculate the Median Absolute Deviation (MAD)
Compute MAD to assess displacement accuracy

8: Store displacements and MAD
Save calculated displacements and MAD values for the current overlap

9: End for
End the loop over overlaps for the current grid

10: Choose the best accurate speckle displacement based on the overlap ending with minimal MAD and store it for the current grid
Select the displacement with the least MAD for the current grid

11: End for
End loop over all grids

12: Generate the displacement map using the best computed speckle displacements for all grids
Create the final displacement map based on the stored best displacements

Return: Displacement map $\boldsymbol{A}$

In the algorithm, the parameter O represents the overlap, which modifies the effective grid size during the calculation of speckle displacement. When an overlap O is introduced, the initial grid size S expands symmetrically in both directions. Specifically, the grid size S increases by a factor of $1 + O$, meaning that the new effective grid size becomes $S(1 + O) \times S(1 + O)$. This expansion happens equally in both the positive and negative directions for each grid.

If O is positive, the effective grid size increases, allowing the algorithm to capture a larger area around the initial grid. This can help detect larger displacements more reliably by incorporating more

surrounding data into the correlation process. Larger effective grids reduce the risk of poor correlation or missed matches when displacements exceed the original grid size. Conversely, if O is negative, the effective grid size decreases. This reduction in effective grid size can enhance the resolution of the algorithm, allowing it to focus on finer details and detect smaller, localized displacements with greater accuracy. Smaller grids provide higher spatial resolution, which is particularly beneficial in detecting subtle deformations that may occur over small regions. By narrowing the area analyzed, the algorithm becomes more sensitive to localized variations in the speckle pattern, improving its adaptability to regions with fine-scale deformation. In both cases, the adjustment happens symmetrically, ensuring that the grid expands or contracts equally in all directions.

By fine-tuning the overlap parameter O, the algorithm dynamically adjusts the effective grid size, allowing it to adapt to the specific scale of the displacement being measured. This adaptability ensures that the algorithm can optimize both the resolution and accuracy of the displacement detection, making it capable of precisely measuring both large-scale and small, localized speckle movements.

2.2. The theory behind image registration and displacements calculation

In the context of detecting displacements between two grids, we employ a Fourier-based image correlation method to implement registration by correlating two images in the frequency domain using FFT [37]. This approach exploits the fact that translation in the spatial domain corresponds to a linear phase shift in the frequency domain, allowing for the accurate detection of displacement vectors [40]. The technique estimates the translation vector between the grids of the reference and deformed images by computing the cross-power spectrum of their Fourier transforms. By taking the inverse Fourier transform of this cross-power spectrum, a correlation matrix is produced, and the peak in this matrix reveals the translation offset between the two grids.

To ensure accuracy and mitigate spectral leakage in the frequency domain caused by periodic extension during FFT, we apply a Blackman window to each grid. This choice is motivated by its superior sidelobe suppression, which reduces spectral leakage more effectively than the Hann or Hamming windows [41]. The Blackman window smoothly tapers intensity values at the grid edges, minimizing abrupt transitions that can introduce artificial high-frequency components, thereby improving the stability of the registration results.

Unlike Hann or Hamming windows, the Blackman window's strong sidelobe attenuation preserves critical frequency content needed for speckle correlation, while reducing phase errors introduced by leakage in the Fourier domain. This is particularly important for broadband signals like speckle patterns, where leakage can significantly distort displacement estimates. Although the Blackman window attenuates edge pixels, we compensate by overlapping grids, ensuring that no information is lost.

$$w(n) = a_0 - a_1\cos\left(\frac{2\pi n}{N-1}\right) + a_2\cos\left(\frac{4\pi n}{N-1}\right), \tag{1}$$

where $w(n)$ is the value of the window function at index n, n is the index along one of the rows or columns of the section, N is the total number of samples in the window, $a_0 = 0.42$, $a_1 = 0.5$, and $a_2 = 0.08$.

Eq. (1) generates the coefficients of the Blackman window, which are then multiplied element-wise with $I(x,y)$, the intensity of the grids at spatial coordinate of (x,y), to apply the windowing effect. Therefore, we have:

$$f_1(x,y) = I_1(x,y).w(x).w(y), \tag{2}$$

$$f_2(x,y) = I_2(x,y).w(x).w(y), \tag{3}$$

where $f_1(x,y)$ and $f_2(x,y)$ are the intensity functions of the reference and deformed grids affected by Blackman window, respectively.

The Fourier transform of the spatial domain grid $f(x,y)$ is

$$F(u,v) = \iint_{-\infty}^{\infty} f(x,y).e^{-2\pi i(ux+vy)}dxdy, \tag{4}$$

where $F(u,v)$ is the Fourier transform of the grid, and u and v are the spatial frequency coordinates.

After the Fourier transform, high-pass emphasis filtering is applied to enhance high-frequency components in the Fourier magnitude spectra while suppressing low-frequency components. This helps improve the robustness of phase correlation by emphasizing image details and reducing the impact of background noise.

To do so, we first obtain Fourier magnitude spectra F_1 and F_2 of the reference and deformed grids, respectively, and apply a high-pass filter $H(u,v)$ to enhance high-frequency components. The enhanced Fourier magnitude spectrum of the fixed and deformed grids become:

$$F'_1(u,v) = |F_1(u,v)|.H(u,v), \tag{5}$$

$$F'_2(u,v) = |F_2(u,v)|.H(u,v), \tag{6}$$

where $H(u,v)=(1 - X(u,v))(2 - X(u,v))$ and $X(u,v)=\cos(\pi u).\cos(\pi v)$.

The cross-power spectrum (P) is then calculated as the complex conjugate of the Fourier transform of one grid multiplied by the Fourier transform of the other grid:

$$P(u,v) = \frac{F'_1(u,v).F'^{*}_2(u,v)}{|F'_1(u,v).F'^{*}_2(u,v)|}, \tag{7}$$

where $F'^{*}_2(u,v)$ denotes the complex conjugate of $F'_2(u,v)$.

The PC operation involves taking the inverse Fourier Transform IFFT of the cross-power spectrum $P(u,v)$ to obtain the correlation matrix $C(x,y)$ in the spatial domain:

$$C(x,y) = \text{IFFT}\{P(u,v)\}. \tag{8}$$

The displacement between the two grids is identified by locating the peak in the correlation matrix $C(x,y)$. The coordinates of this peak indicate the horizontal and vertical shifts required to align the grids.

$$(\Delta x, \Delta y) = \arg\max_{(x,y)} C(x,y), \tag{9}$$

where $(\Delta x, \Delta y)$ are the detected displacements.

3. Simulation study and optimization

3.1. Numerical simulation

In this study, we simulate laser speckle patterns to evaluate the performance of the proposed method for speckle displacement measurement. To generate speckle patterns, we use a numerical approach that creates a random phase matrix combined with a uniform amplitude field representing the laser beam. The resulting complex field undergoes a Fourier transform to produce the speckle pattern. In cases where it is necessary to manipulate the speckle size, an optional zero-padding step can be applied before the Fourier transform. This increases the speckle size and allows for studying larger displacements or reducing high-frequency noise. After applying zero-padding, the central region of the transformed speckle pattern can be extracted to match the desired size.

The generated speckle pattern is then used as the reference image I_{ref} in our algorithm, while known local displacements are introduced into different areas of I_{ref} to create the deformed image I_{def}. These displacements vary in both magnitude and affected area, ranging from minute, localized deformations to larger-scale shifts across different regions. By applying these controlled displacements to both small and large areas, we can evaluate whether the proposed algorithm accurately detects and measures both subtle, localized deformations and larger-scale displacements in regions of varying size. This allows us to thoroughly investigate the algorithm's robustness and accuracy across different

scales of displacement.

Algorithm 2
Adaptive Resolution Grid-Based Phase Correlation for Speckle Displacement Measurement.

Input:
- Speckle pattern image size: N
- Zero-padding size (optional): N_{pad}

Output:
- Speckle pattern: $I_{speckle}$

1: Initialize parameters
Set pattern size N
Set padded size N_{pad}

2: Generate a random phase matrix
Create a matrix of random phases:
Random Phase=rand(N,N)×2π
Randomly distributed between 0 and 2π

3: Create a uniform amplitude field
Set Amplitude Field=ones(N,N)

4: Combine amplitude and phase to form a complex field
Compute complex field:
Complex Field= Amplitude Field $\times e^{i\times \text{Random Phase}}$

5: Perform Fourier transform (with optional zero-padding)
If zero-padding is used:
Speckle Pattern = $|fftshift(fft2(Complex\ Field,\ [Npad,\ Npad]))|^2$

If no zero-padding is used:
Speckle Pattern = $|fftshift(fft2(Complex\ Field,\ [N,\ N]))|^2$
Skip Step 6 and proceed to Step 7.

6: (Optional) Extract the central region if zero-padding is used
Select a central region with the desired size
Extract Center Region from the padded speckle pattern

7: Normalize the extracted speckle pattern
Normalize to maximum intensity value 1:
$Speckle\ Pattern = \frac{Speckle\ Pattern}{\max(Speckle\ Pattern\ (:))}$

8: Output the normalized speckle pattern
Return $I_{speckle}$ = *Speckle Pattern*

Return: Speckle pattern $I_{speckle}$

To evaluate the performance of our proposed adaptive resolution grid-based phase correlation algorithm, we first generated a 600 × 600 pixel speckle pattern image as the reference image I_{ref}. Displacements were then introduced into five distinct regions of the reference speckle pattern to create the deformed image I_{def}, as shown in Fig. 1. The regions affected by the displacements are highlighted by squares in the figure, with the speckle patterns before and after the shifts displayed on the left and right, respectively.

The specific sizes of each region and their corresponding displacement values are as follows:

- Upper-Left Corner (Region 1), 250 × 250 pixels:
  - **X-direction shift:** 20 pixels to the right.
  - **Y-direction shift:** 18 pixels upward
- Upper-Right Corner (Region 2), 60 × 60 pixels:
  - **Y-direction shift:** 6 pixels downward
- Center of the image (Region 3), 40 × 40 pixels:
  - **X-direction shift:** 4 pixels to the right
  - **Y-direction shift:** 4 pixels downward
- Bottom-Left side of the image (Region 4), 50 × 50 pixels:
  - **X-direction shift:** 5 pixels to the right
  - **Y-direction shift:** 6 pixels upward
- Bottom-Right Corner (Region 5), 30 × 30 pixels:
  - **X-direction shift:** 4 pixels to the right
  - **Y-direction shift:** 4 pixels downward

These controlled displacements allow us to evaluate the proposed method's ability to detect and measure displacements across regions of varying sizes and magnitudes. The simulation includes both subtle, localized deformations and larger-scale shifts, testing the method's

robustness and adaptability. By applying varying displacement magnitudes and region sizes, we thoroughly assess the method's capacity to resolve different displacements while adapting to the size of the affected regions.

In this section, we investigate how varying grid sizes S and overlap O influence the accuracy of the proposed method in detecting displacements of different magnitudes across regions of varying sizes within the image. Fig. 2 shows the results for a grid size of 30 × 30 pixels, with overlap values of 1, 2, 4 and 6 (Fig. 2a, 2b, 2c, and 2d, respectively). Similarly, Fig. 3 displays the results for a grid size of 20 × 20 pixels, and Fig. 4 presents the results for a grid size of 15 × 15 pixels, each with overlap values of 1, 2, 4 and 6, respectively.

As seen in Figs. 2–4, when the effective grid size $S(1 + O)$ becomes significantly larger than the deformed area or displacement magnitude, the algorithm struggles to detect shifts accurately. Conversely, when the effective grid size is considerably smaller than the deformed region, the algorithm can still detect the deformed area but fails to accurately compute the displacement values.

These results highlight the crucial role of the overlap parameter O in detecting displacements. In the simulated case, the displacement magnitudes and deformed area sizes are predetermined, allowing us to evaluate the method's performance across various scenarios. In real-world applications, however, the deformed regions and displacements are unknown, making the choice of grid size and overlap critical for robust detection.

One potential solution, demonstrated in Figs. 2–4, is to systematically vary the grid size and overlap while observing the resulting displacement maps. This approach helps to identify configurations where the displacement vectors (represented by arrows) within each local deformed regions exhibit consistent and logical behavior in both size and direction. Based on our analysis, the configuration with a grid size of 15 × 15 pixels and an overlap of 4 emerges as the most effective overall for this particular example, and could serve as a reference for selecting optimal grid and overlap parameters.

Next, we focus on the performance of the algorithm in Fig. 4c, analyzing its effectiveness for each local deformed region in detail.

Fig. 5a provides a zoomed-in view of Region 1 from Fig. 4c, showing that the computed shifts U and V accurately match the actual displacements introduced in the simulation. It is worth noting that in MATLAB, the sign of V (in the data box) is printed opposite to the conventional Y-direction; however, the arrows correctly represent the direction of the introduced shifts. Blue points represent the center of each grid.

In Fig. 5b, we zoom in on Region 2 from Fig. 4c, where the computed displacements closely match the actual shifts. Fig. 5c shows similar accuracy in Region 3. In Fig. 5d, the displacement vectors for the bottom-left region (Region 4) of Fig. 4c are displayed, further confirming the method's capability. Finally, Fig. 5e shows the computed displacements for the bottom-right region (Region 5) of Fig. 4c, where a high degree of correspondence is observed between the computed and actual shifts.

Although the grid size of 15 × 15 pixels and the constant overlap value of 4 produce strong accuracy across the regions, there remains room for further refinement. Rather than applying a constant effective grid size across the entire image, we propose that the effective grid size be adaptively adjusted and optimized for each grid during the computation of displacements. This approach would allow the algorithm to fine-tune its performance based on the local deformation characteristics.

3.2. Adaptive resolution with dynamic and automatic overlap optimization

An effective approach for achieving adaptive resolution is to dynamically adjust the overlap value for each grid during computation. Instead of applying a single overlap value across the entire image, the algorithm tests a range of overlaps for each local region to identify the optimal overlap size. This allows the algorithm to adapt to various scales of deformation across regions, which may differ both in size and

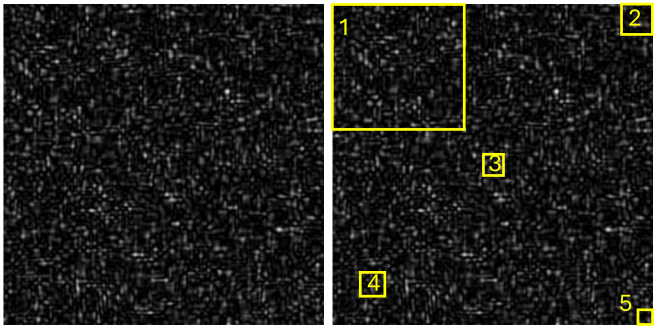

Fig. 1. Speckle patterns before (left) and after (right) the introduction of controlled displacements. Five distinct regions, highlighted by squares, show varying displacement magnitudes and region sizes. The regions represent different scales of deformation used to evaluate the method's performance in detecting both subtle and larger displacements.

displacement characteristics, some regions might be small with subtle shifts, while others could be larger with more pronounced deformations.

Initially, we explored using correlation-based metrics to optimize the overlap. However, due to inherent image noise, these methods often favored larger overlaps (larger effective grids) because stronger correlation values were achieved, albeit at the cost of reduced resolution. This approach led to suboptimal results in areas where high resolution was needed. To overcome this, we investigated alternative metrics and found that MAD provided superior resilience. Compared to mean-based methods, MAD offers a more robust measure of central tendency, being less affected by outliers. This made MAD better suited for determining the optimal overlap size, maintaining both accuracy and resolution.

By continuously adjusting the overlap O during the computation and using MAD as the guiding metric, the algorithm dynamically selects the most appropriate effective grid size and overlap for each region. This results in an automatic and adaptive resolution that can handle deformed regions with different sizes and deformation characteristics, maintaining accuracy without sacrificing resolution. MAD, calculated as:

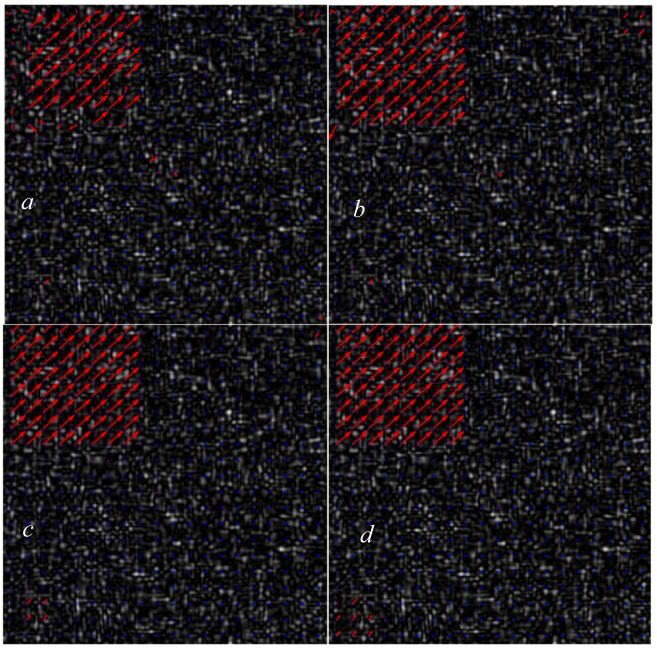

Fig. 2. Displacement vectors for a grid size of 30 × 30 pixels with overlaps of 1, 2, 4, and 6 in (a)–(d), respectively.

$$MAD = median(|\varepsilon_i - median(\varepsilon)|), \tag{10}$$

where ε_i represents residual (the pixel-wise difference) between two grids after the alignment which is calculated as:

$$\varepsilon_i = I_1(x,y) - I'_2(x,y), \tag{11}$$

where and $I_1(x,y)$ represents the intensity value at position (x, y) in the selected grid from the reference image, while $I_2(x,y)$ is the intensity value from the corresponding grid found in the deformed image. And $I'_2(x,y)$ refers to the intensity values of the corresponding grid in the deformed image after it has been geometrically transformed and aligned with the reference grid using the computed displacements $(\Delta x, \Delta y)$. This transformation ensures that the two grids are aligned and comparable. The $median(\varepsilon)$ represents the median residual of all pixel intensity differences between the two aligned grids.

Thus, we directly measure the residual errors after alignment, providing a reliable indication of the registration accuracy. The MAD of the residuals between the reference grid and the transformed grid serves as critical feedback for the optimization process. It determines whether the chosen transformation parameters, including the overlap value, yield a precise alignment. This metric ensures that the algorithm adjusts dynamically to find the optimal overlap (Consequently optimal effective grid size) for each region, based on the actual deformation characteristics.

To evaluate this optimization method, we used a fixed grid size of 15 × 15 pixels and varied the overlap range O from 0 to 5, incrementing by 0.2 (i.e., 0:0.2:5). The results of this evaluation are shown in Fig. 6. As seen, the detected speckle displacements are highly accurate, with arrows representing the detected shifts clearly covering all local deformed regions. These areas exhibit different deformation characteristics, yet the algorithm successfully adapts to varying overlap values and captures both small and large displacements with high accuracy.

To analyze the results in greater detail, we focus on the different regions of Fig. 6, as done in previous sections, to investigate the computed displacements.

In Region 1, illustrated in Fig. 7*a*, the computed displacements align perfectly with the actual shifts. For Region 2, the zoomed-in view in Fig. 7*b* demonstrates that the computed displacements accurately reflect

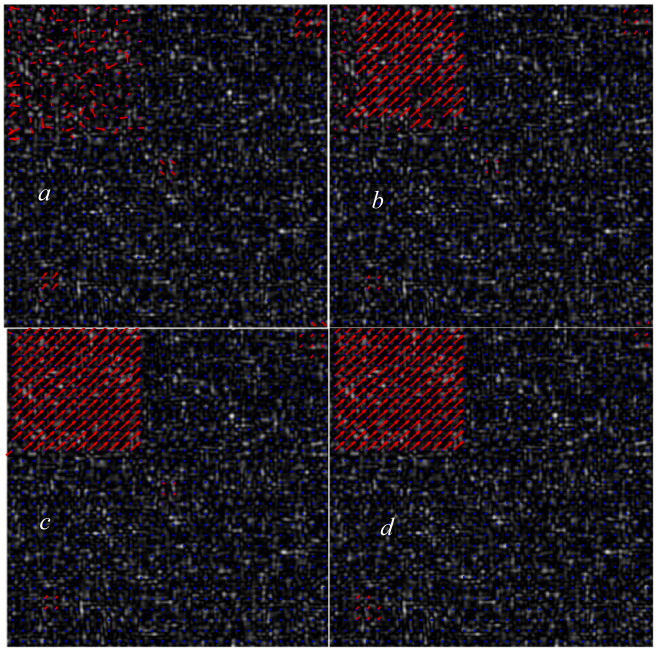

Fig. 3. Displacement vectors for the grid sizes of 20 × 20 pixels with overlaps of 1, 2, 4, and 6 in (a)–(d), respectively.

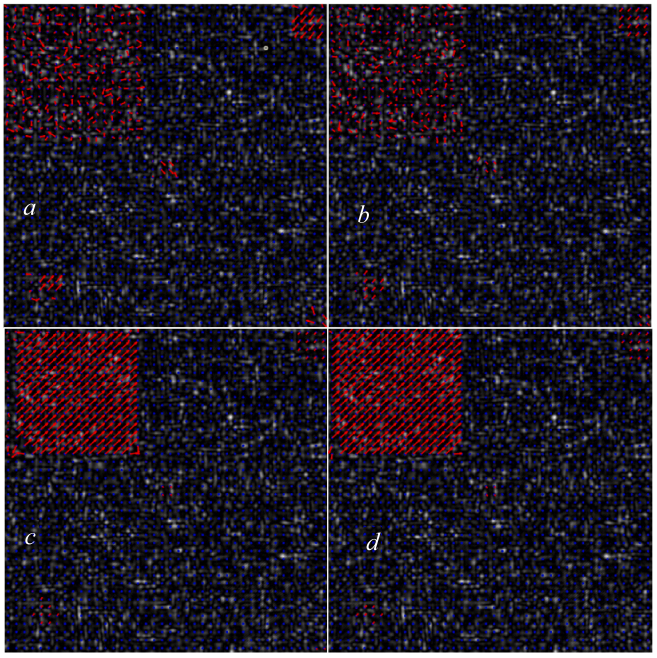

Fig. 4. Displacement vectors for the grid sizes of 15 × 15 pixels with overlaps of 1, 2, 4, and 6 in (a)–(d), respectively.

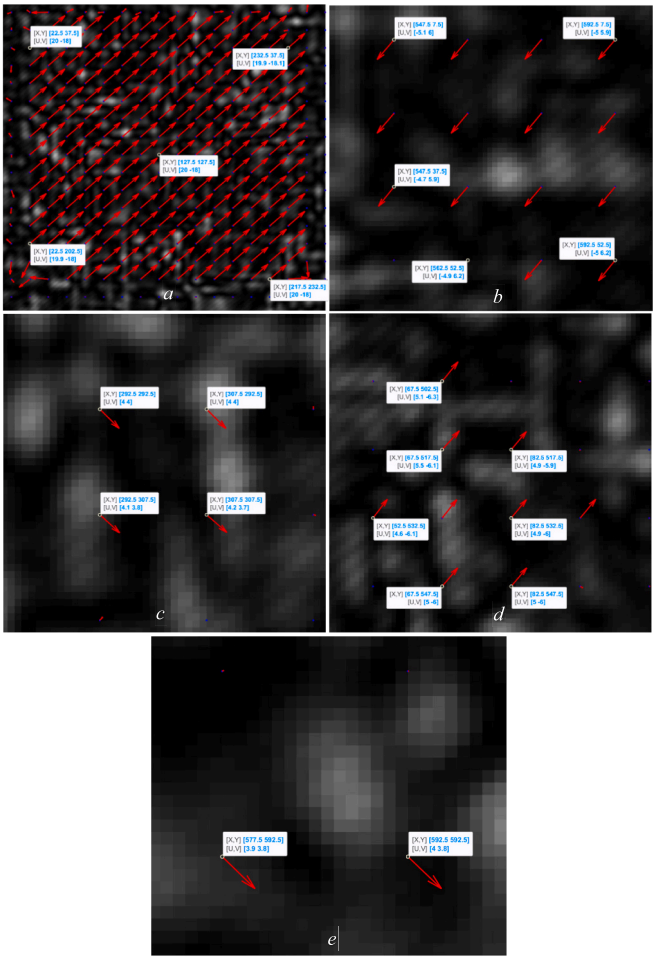

Fig. 5. Fig. 4*c* zoomed with displacement details in *a*: Region 1, *b*: Region 2, *c*: Region 3, *d*: Region 4, *e*: region 5.

the actual shifts. Similarly, the center region of Fig. 6, as shown in the zoomed-in view in Fig. 7*c*, also reveals an accurate match between the computed and actual displacements. Moving on to Region 4, as seen in Fig. 7*d*, the computed displacements again correspond to the actual shifts. Lastly, in the zoomed-in view of Region 5 shown in Fig. 7*e*, we observe a strong alignment between the actual and computed displacements, with only minimal differences.

Upon analyzing Fig. 7, it is evident that the computed displacements align more accurately with the actual displacements compared to the results seen in Fig. 4. Notably, the optimization method eliminates the misalignment issues previously observed in Figs. 2–4, where arrows occasionally pointed in incorrect directions. Specifically, the detected speckle displacement using the best manually set (fixed resolution) method – shown in Fig. 4c, yielded relative errors of 15.2 % and 15.17 % in Region 1 for the X and Y directions, respectively. For Region 2, the relative errors were 0.4 % in the X direction and 1.5 % in the Y direction. In Region 3, the relative errors were 1.75 % for X and 3 % for Y. Region 4 exhibited relative errors of 5 % in the X direction and 0.8 % in the Y direction, and Region 5 showed relative errors of 1.25 % for X and 5 % for Y.

In contrast, with the proposed optimized (adaptive resolution) method, the relative error rates decreased significantly (Fig. 6). In Region 1, the relative errors dropped to 1.35 % in the X direction and 1.28 % in the Y direction. For Region 2, the errors were 0 % in both X and Y directions. In Region 3, the errors reduced to 1.25 % in both X and Y directions. Region 4 showed error rates of 1 % and 0.8 % in X and Y directions. Region 5 achieved errors of 2.5 % in both X and Y directions. The optimization approach has therefore successfully enhanced the accuracy and consistency of the displacement detection across all regions.

To further illustrate the effectiveness of the dynamic and automatic overlap optimization approach, we plot the MAD values as a function of the overlap O for five representative grids, each selected from Regions 1 to 5. These regions exhibit varying deformation characteristics, with differences in both the size of the deformed area and the magnitude of the displacement, which necessitate different resolutions to accurately detect the local displacements.

Fig. 8 presents the results of this analysis. For a grid in Region 1, which corresponds to a larger deformed area, the MAD reaches its minimum value at an optimal overlap of $O = 3.2$. In contrast, for Region 2, which is characterized by a smaller deformation area, the optimal overlap is $O = 2.4$. The displacement in Region 3, located near the center of the image, requires a significantly smaller overlap of $O = 0.6$ to minimize the MAD value. Meanwhile, in Region 4, the optimal overlap is found to be $O = 1.2$, and for Region 5, the MAD reaches its minimum at $O = 1.8$. These results demonstrate the algorithm's ability to adaptively select different overlap values based on the unique deformation characteristics of each region, ensuring optimal detection of displacements across a wide range of scales and conditions.

4. Experimental validation

In this section, we further validate the proposed adaptive resolution speckle displacement measurement method through two distinct experiments: controlled deformations using a micrometer translation stage, and uncontrolled deformations induced by random forces applied to a cardboard surface. These experiments are designed to assess the algorithm's robustness and effectiveness in detecting both known and unknown displacements under different conditions.

4.1. Controlled deformations using a micrometer translation stage

4.1.1. Experimental setup

In the controlled deformation experiment, we employed a green laser to generate coherent light, which was then directed onto a cardboard surface. A diffuser lens was used to scatter the laser beam, ensuring uniform illumination across the surface. The scattered laser light produced a speckle pattern on the cardboard, which was captured by a digital camera equipped with an objective lens.

To induce controlled displacements, we mounted the cardboard on a micrometer translation stage, which allowed precise movement in both the X and Y directions. The micrometer translation stage used in the experiment had a resolution of 10 μm. The experimental setup is shown in Fig. 9, with the left image showing the schematic of the setup and the right image displaying the real equipment.

4.1.2. Controlled translation procedure

The experiment began by capturing a reference speckle image of the cardboard surface. The object was then manually displaced using a micrometer translation stage, which allowed for controlled movements in both the X and Y directions. The displacements were applied as follows:

(X = 0 μm, Y = 50 μm)
(X = 100 μm, Y = 150 μm)
(X = 200 μm, Y = 200 μm)
(X = 250 μm, Y = 500 μm)

After each displacement, the corresponding speckle images were captured and analyzed using the developed speckle displacement measurement algorithm. The extracted speckle displacement fields for each controlled translation are presented in Fig. 10, consisting of four subfigures representing different translation cases.

In Fig. 10*a*, the computed displacements are shown for the micrometer shift of (X = 0 μm, Y = 50 μm). Fig. 10*b* illustrates the computed displacements for a shift of (X = 100 μm, Y = 150 μm). In Fig. 10*c*, the computed displacements are shown for a shift of (X = 200 μm, Y = 200 μm), and Fig. 10*d* corresponds to the largest translation of (X = 250 μm, Y = 500 μm).

In each subfigures of Fig. 10, the red arrows represent the computed displacement vectors, indicating the detected shifts across the speckle field. It is important to note that while the direction of the arrows is accurate, their length has been automatically scaled by MATLAB for visualization purposes, and does not directly correspond to the actual displacement values. To ensure the true displacement magnitude is accurately conveyed, each subfigure includes a data box. This data box provides specific computed displacement values at a given point in the field, displaying the calculated shifts (μm) in the X (U) and Y (V) directions.

4.1.3. Results and analysis

The proposed adaptive resolution speckle displacement measurement algorithm was applied to the captured images for each controlled translation. The measured displacements were compared with the

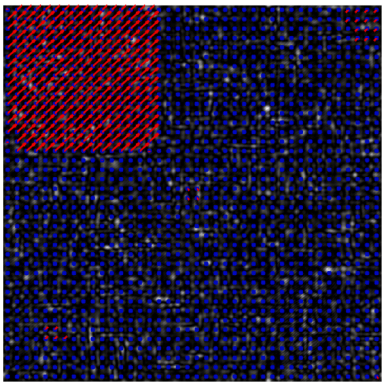

Fig. 6. Detected optimal displacement vectors using a grid size of 15 × 15 pixels with dynamically optimized overlap, demonstrating adaptive resolution across different regions.

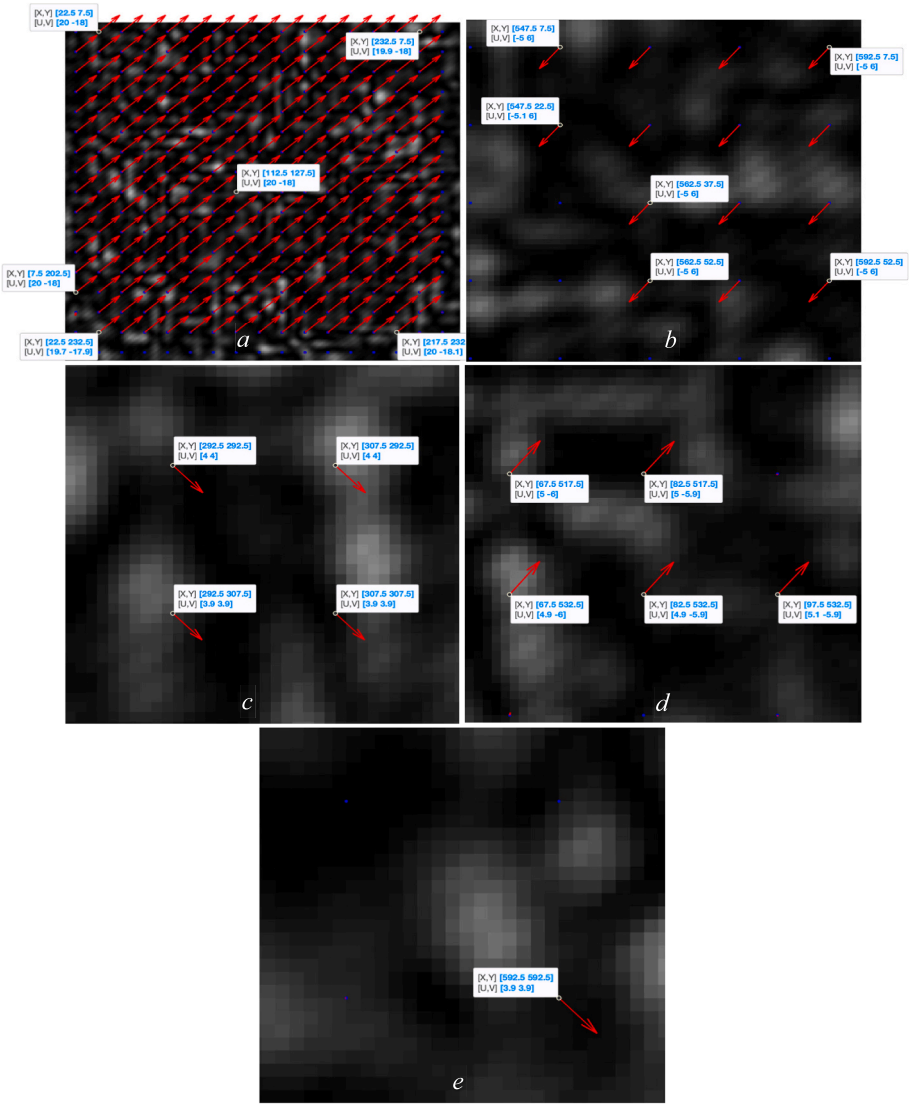

Fig. 7. Detected optimal displacements after optimization (Fig. 6 Zoomed) in *a*: Region 1, *b*: Region 2, *c*: Region 3, *d*: Region 4, *e*: region 5.

known displacements introduced by the manual micrometer translation stage. Table 1 summarizes the actual displacements in micrometers (μm) alongside the systematic and random errors in the displacement values calculated by the algorithm. It also includes the relative systematic error as a percentage for both X and Y directions. Overall, the results indicate that the algorithm accurately tracks the speckle displacements, with generally low error rates across different translations. This confirms the robustness and effectiveness of the method in detecting and measuring controlled speckle displacements.

Upon closer inspection of the results, differences were observed between displacements measured in the upper and lower parts of the image, as well as between the rightmost and leftmost parts. For instance, for an actual shift of (X = 0 μm, Y = 50 μm), the measured Y displacement in the upper part of the image was 54.95 μm, while in the lower part, it was 51.62 μm. Similarly, for X displacement in the same test, the average measured shift in the most upper part of the image was 1.52 μm, while in the lowest part, it increased to 2.49 μm. Despite no actual displacement in the X direction, the systematic error of 1.6 μm suggests a slight drift in the experiment, which contributes to a higher error rate in X compared to Y in subsequent translations.

These discrepancies suggest that the cardboard surface may not be perfectly aligned with the X-Y plane of the camera's field of view, leading to slight inclinations. Even small inclinations of the surface along both the X and Y axes can introduce out-of-plane displacements, affecting the accuracy of the measured shifts. This is especially evident in regions where the speckle movement is most sensitive to such angular misalignments. The systematic difference between the upper and lower areas of the image supports this hypothesis.

Moreover, these factors, along with the manual operation of the micrometer translation stage, which has a resolution of 10 μm, introduce further uncertainty. Human-induced variations, combined with the mechanical limitations of the translation stage, contribute to the observed error rates. These uncertainties and limitations become more significant when measuring smaller actual displacements, where the errors become comparable to the size of the displacement itself. This is why minute displacements are more affected by these errors.

To minimize these sources of error and improve measurement accuracy, further calibration of the system could be performed in future work. Additionally, employing a motorized micrometer translation stage would also minimize human variability, improving the consistency of the translations and further refining the accuracy of the displacement measurements.

4.2. *Uncontrolled deformations: Random speckle movements*

In the second experiment, we tested the algorithm's robustness in

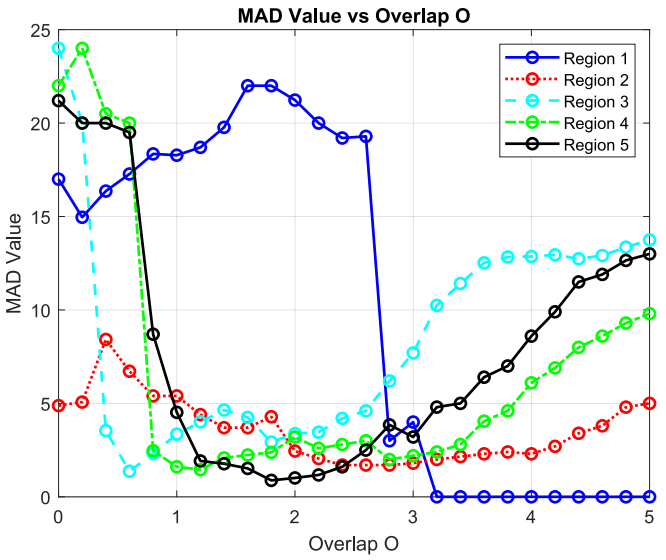

Fig. 8. Plot of MAD values as a function of overlap O for representative grids from Regions 1 to 5. The optimal overlap varies across regions, reflecting the algorithm's ability to adapt to different deformation area sizes and displacement magnitudes, with minimum MAD values indicating the most accurate alignment for each region.

detecting random, uncontrolled deformations. In this case, speckle displacements were introduced by spraying water onto a cardboard surface, creating random shifts in the speckle pattern. The setup and camera remained the same as in the previous experiment. We aimed to experimentally track the displacement of surface speckles on the cardboard surface over time after it was sprayed with water. The cardboard surface was initially dry, and water droplets were distributed randomly across the surface using a fine mist spray bottle. After spraying the surface with water, a sequence of speckle images was captured to observe the temporal changes in the speckle pattern over time. Unlike the controlled experiment, the exact amount of displacement caused by the water spray was unknown, making this a more challenging scenario for the algorithm. The speckle pattern formed on the surface of the cardboard under laser illumination is shown in Fig. 11.

The proposed algorithm was applied to track the speckle displacements resulting from the random deformations and are shown in Fig. 12. Despite the uncontrolled nature of the deformations, the algorithm successfully detected the displacements across different areas of the image. The effectiveness of the adaptive resolution approach allowed for the simultaneous detection of minute, subtle, and large displacements, even in regions where the deformation was unevenly distributed.

The movement of the speckles was primarily due to the interaction between the water and the cardboard surface. When water was sprayed onto the cardboard, the spreading and absorption of the water caused temporal changes in the speckle pattern. These changes were detected as displacements in the speckle positions between the two images. The speckle pattern shifted because the scattering properties of the cardboard surface were altered by the movement of water, which resulted from water absorption, expansion, spreading, and evaporation. The displacement vectors of the speckles provided quantitative information about surface deformation and the dynamics of water absorption and evaporation.

5. Discussion

The adaptive resolution grid-based phase correlation algorithm introduced in this study offers a significant advancement in speckle displacement measurement, providing enhanced precision in surface deformation analysis for optical metrology and non-destructive testing (NDT). Traditional correlation techniques typically divide the entire image into fixed sub-images (grids) to detect displacements. However, these sub-images are static in size, which presents limitations when the scale of deformation varies across different regions of the image. Fixed sub-images often fail to capture the full range of displacement characteristics, small grids may not detect large displacements effectively, while large grids may overlook minute, localized deformations. The challenge lies in achieving the right balance between resolution and robustness for varying deformation scales.

In our algorithm, we address this challenge by introducing the concept of *effective grids* (or *effective sub-images*), which are dynamically adjusted based on local deformation characteristics. This is achieved through the introduction of an overlap parameter (O). The overlap, when combined with the initial grid size (S), forms the effective grid size $S(1 + O)$, allowing the algorithm to adaptively adjust the sub-image dimensions. Unlike conventional methods where the sub-image size is fixed throughout the entire image, our approach allows the effective grid size to vary, ensuring better adaptability to both small and large displacements within regions of different sizes.

This dynamic adjustment is key to the algorithm's success, as it enables the detection of all types of deformations, subtle, minute, or large-scale, without sacrificing resolution. By adjusting the overlap for each grid independently, the algorithm captures a broader range of deformation characteristics, providing a significant improvement over static methods that require manual tuning of grid sizes. This automated approach ensures high accuracy in detecting both localized fine displacements and larger-scale deformations.

While the adaptive grid sizing enhances the ability to capture both fine and large-scale deformations, the fundamental resolution of displacement measurements remains governed by the sensor's pixel pitch, the speckle grain size, and the quality of the correlation. In practical terms, reliable displacement tracking requires speckle grains to span multiple pixels, typically 3 to 5, to ensure sufficient intensity variation and avoid aliasing [42,43]. Although subpixel algorithms are capable of detecting displacements at sub-pixel levels, maintaining precision depends critically on the presence of adequately sized speckles and well-textured correlation grids. Smaller grids improve spatial

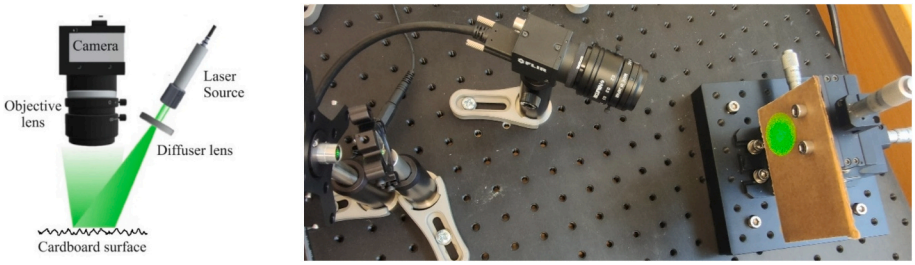

Fig. 9. Schematic (left) and actual arrangement (right) of the experimental system. The setup includes a green laser source, a diffuser lens, and a digital camera for capturing speckle patterns. The cardboard, serving as the targeted test object, is mounted on a micrometer translation stage for precise displacements. (For interpretation of the references to colour in this figure legend, the reader is referred to the web version of this article.)

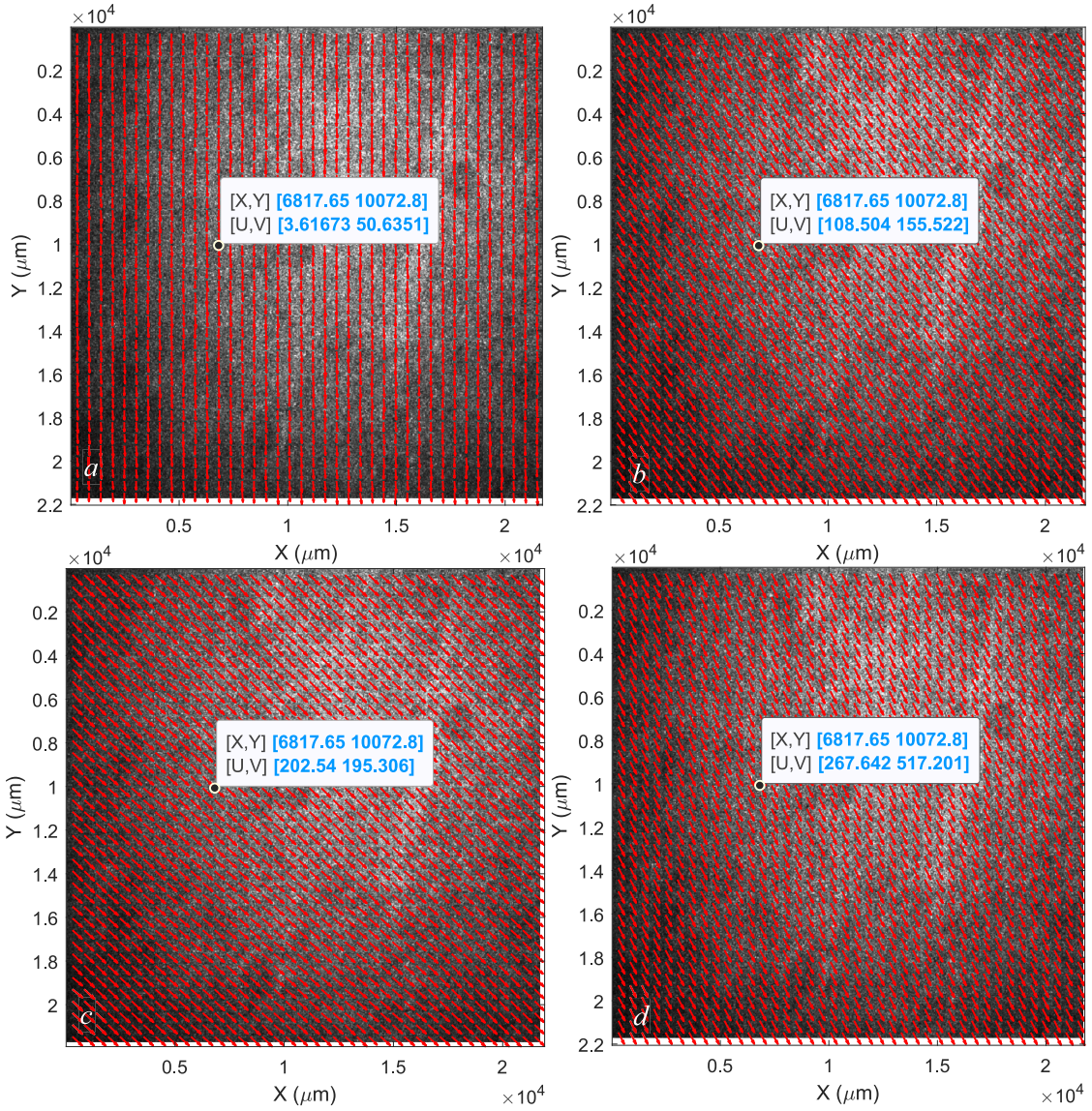

Fig. 10. Computed displacement fields for controlled translations of the cardboard surface: (X = 0 μm, Y = 50 μm) (*a*), (X = 100 μm, Y = 150 μm) (*b*), (X = 200 μm, Y = 200 μm) (*c*), and (X = 250 μm, Y = 500 μm) (*d*). Red arrows represent the computed displacement vectors, scaled for clarity. Data boxes indicate the actual computed displacements (U, V) in μm at a specific point. (For interpretation of the references to colour in this figure legend, the reader is referred to the web version of this article.)

Table 1
Summary of controlled displacements produced by a manual micrometer translation stage and the corresponding systematic and random errors measured by the speckle displacement measurement algorithm, with relative systematic error reported for each translation in the X and Y directions.

Actual Displacement (μm)	Systematic Error (μm)	Random Error (μm)	Relative Systematic Error (%)
X = 0, Y = 50	X = 1.6, Y = 0.16	X = 1.89, Y = 7.32	X = N/A, Y = 0.32 %
X = 100, Y = 150	X = 7.82, Y = 8.06	X = 1.48, Y = 3.43	X = 7.82 %, Y = 5.37 %
X = 200, Y = 200	X = 8.37, Y = −1.12	X = 8.6, Y = 7.96	X = 4.19 %, Y = −0.56 %
X = 250, Y = 500	X = 16.88, Y = 18.2	X = 11.54, Y = 10.35	X = 6.75 %, Y = 3.64 %

resolution but may reduce measurement precision if they contain too few speckle features, while larger grids provide more stable correlation at the cost of local detail. The adaptive nature of the proposed method helps mitigate this trade-off by adjusting grid overlap and size based on local deformation complexity, maintaining high tracking performance across varying regions of the image.

Moreover, we combined our algorithm with phase correlation (PC) due to its unique advantages over other correlation techniques. PC provides robustness against global variations in contrast and brightness, offering sharper and more stable correlation peaks [36]. This makes it particularly effective in noisy environments where other techniques may struggle. By incorporating PC into our adaptive resolution algorithm, we benefit from these strengths, enabling accurate displacement detection even in conditions with high-frequency noise. The combination of PC and our dynamic overlap approach ensures superior performance compared to traditional intensity-based or global correlation techniques.

5.1. *Effective grid size and overlap*

The effectiveness of the algorithm relies heavily on the interplay between the grid size (*S*) and the overlap parameter (*O*). In conventional

methods, the grid size is fixed, which often leads to compromises in accuracy when dealing with varying deformation magnitudes. In our approach, the overlap modifies the effective grid size dynamically, providing the flexibility to adapt the resolution as needed.

- Positive Overlap ($O > 0$)**:** When the overlap is positive, the effective grid size increases. This helps the algorithm capture larger displacements by incorporating more surrounding data into the correlation process, thereby reducing the risk of poor correlation or missed matches when displacements exceed the original grid size. Larger effective grids are particularly useful for detecting broad, large-scale deformations.
- Negative Overlap ($O < 0$)**:** Conversely, when the overlap is negative, the effective grid size decreases. This reduction enhances the spatial resolution of the algorithm, making it more sensitive to smaller, localized displacements. Smaller grids are especially beneficial in detecting subtle deformations that occur over small regions, where high resolution is essential for capturing fine details.

Given that the size of the deformed regions and displacement magnitudes are typically unknown in practical applications, it is advisable to initially select a small grid size to ensure high-resolution detection. Therefore, only positive overlap ($O > 0$) is necessary to increase the effective grid size where larger displacements occur, allowing the algorithm to detect both small and large deformations without the need for negative overlaps.

This dynamic adjustment of the effective grid size ensures that the algorithm can maintain both accuracy and resolution across different scales of displacement. The adaptability provided by the overlap parameter allows the algorithm to optimize its performance based on the specific deformation characteristics in each grid, which is particularly important in real-world applications where the size of the deformed regions and the magnitude of displacements are often unknown.

5.2. *MAD-based optimization*

To further enhance the accuracy of displacement detection, we incorporated a statistical optimization technique based on the median absolute deviation (MAD) of residuals. This optimization method dynamically selects the most appropriate overlap for each grid, refining the effective grid size to best suit the local deformation characteristics. The MAD criterion is particularly effective and more robust against outliers compared to traditional correlation maximization techniques, which tend to favor larger grid sizes that can obscure fine details. By focusing on the residual differences after alignment, MAD ensures that both subtle and larger displacements are accurately detected, without noise masking smaller deformations.

Using MAD as the guiding metric allows the algorithm to avoid the pitfalls of larger grids that often smooth over small deformations. This approach ensures that even minute displacements are detected with high accuracy, making the algorithm resilient to variations in displacement scales.

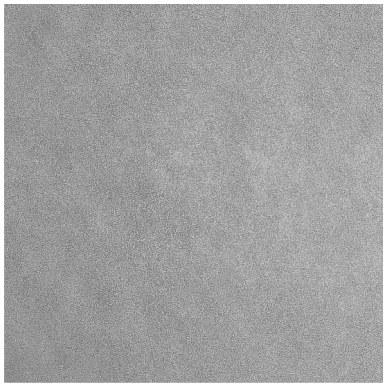

Fig. 11. Speckle patterns observed on the surface of the cardboard under laser illumination.

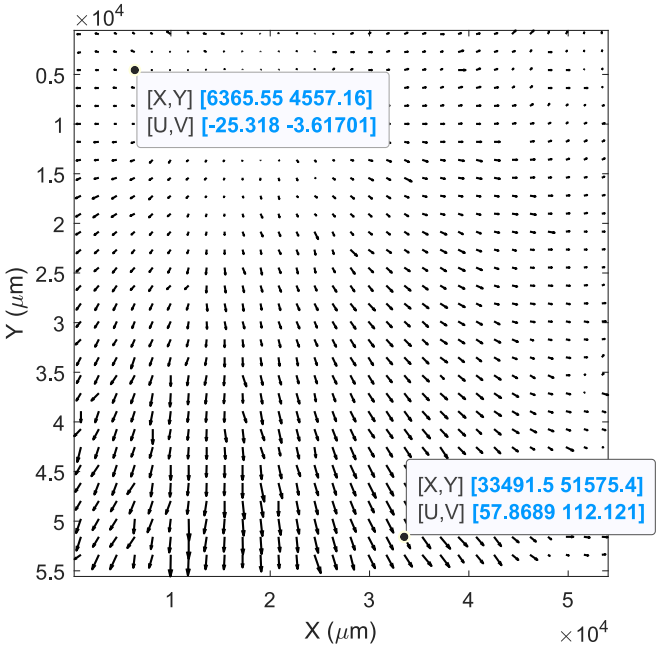

Fig. 12. The surface of the cardboard was randomly sprayed with water. Speckle displacements map showing the temporal changes in the speckle pattern of water sprayed surface.

5.3. *Automatic grid size adjustment*

The core strength of our algorithm lies in its ability to automatically adjust the effective grid size throughout the image. Unlike conventional methods that rely on manual tuning or fixed grid sizes, our algorithm adjusts the overlap dynamically to achieve the optimal balance between resolution and robustness. This ensures that each grid is appropriately sized based on the local deformation characteristics.

For most practical applications, we used symmetrical adjustments in both the X and Y directions. However, in cases where the deformation components in one direction are significantly larger than in the other, a non-symmetrical adjustment may be necessary. For example, if the deformation in the Y direction is dominant, a square grid could lead to inaccuracies in the X direction. In such cases, adjusting the grid size unequally in the X and Y directions would allow for more accurate detection of displacements in both directions. This refinement is particularly important in scenarios where the deformation field is highly anisotropic.

5.4. *Real-world validation and challenges*

The proposed algorithm was validated through both numerical simulations and experimental measurements. In the simulations, controlled displacements were applied to speckle patterns to test the algorithm's ability to detect deformations across regions of different sizes and magnitudes. In the experimental validation, we tested controlled displacements, introduced using a micrometer translation stage, and random deformations induced by spraying water on a cardboard surface. In both cases, the algorithm successfully tracked the displacements, confirming its robustness and adaptability in real-world scenarios.

However, even with this robust optimization method, caution must be exercised when selecting the range of overlap values. Excessively

large effective grid sizes may miss smaller deformations, while overly small grids could result in poor detection of larger displacements. Therefore, the selection of a suitable overlap range is critical to ensuring the algorithm produces the desired range of resolutions across a wide range of deformation magnitudes.

5.5. *Future considerations and enhancements*

In future developments, the algorithm could be extended to handle other types of deformations beyond translations, such as local rotations. While the current implementation focuses on translational shifts, incorporating the ability to detect additional types of deformations would significantly broaden the algorithm's applicability.

Additionally, further exploration of non-symmetrical grid size adjustments for highly anisotropic deformation fields would improve the accuracy of the method, particularly in cases where deformations occur with significantly different magnitudes along the X and Y directions. This refinement would ensure that smaller components of deformation are not missed in the presence of dominant larger components.

Even with MAD-based optimization, there remains a slight degree of residual error. Therefore, future research could consider investigating alternative optimization techniques to further enhance accuracy. Exploring other statistical optimization methods or hybrid approaches may help reduce these errors in specific cases. Additionally, the integration of machine learning or artificial intelligence (AI) [44,45] could provide dynamic grid size and overlap adjustments based on learned data patterns, potentially enhancing performance in real-time, especially in more complex deformation fields.

Finally, the use of a motorized translation stage and improved calibration techniques would enhance further the accuracy of experimental measurements, reducing manual errors and ensuring more accurate displacement measurement in future experiments.

6. Conclusion

In summary, the adaptive resolution grid-based phase correlation algorithm presents a flexible and robust solution for speckle displacement measurement in optical metrology. By combining phase correlation with the introduction of dynamic overlap and effective grid size, the algorithm adapts to both small and large deformations across regions of varying sizes. This adaptability ensures that the method remains accurate in both high-resolution, small-scale deformations and larger-scale displacements, achieving a relative error reduction of up to 14 % compared to the best results obtained with manually fixed grid sizes. The combination of phase correlation with these adaptive features not only makes the method robust, even in noisy environments, but also ensures stable detection of displacement vectors.

The use of MAD-based optimization further refines the algorithm, making it resilient to outliers and capable of detecting fine details without sacrificing robustness. Future work should explore extending the method to detect other types of deformations, such as local rotations, and optimizing the grid size asymmetrically for highly anisotropic deformation fields.

CRediT authorship contribution statement

Hamed Sabahno: Writing – review & editing, Writing – original draft, Visualization, Validation, Software, Methodology, Investigation, Formal analysis, Data curation. **Satyam Paul:** Writing – review & editing, Validation, Software, Data curation. **Davood Khodadad:** Writing – review & editing, Writing – original draft, Visualization, Validation, Supervision, Software, Resources, Project administration, Methodology, Investigation, Funding acquisition, Formal analysis, Data curation, Conceptualization.

Declaration of competing interest

The authors declare that they have no known competing financial interests or personal relationships that could have appeared to influence the work reported in this paper.

Acknowledgments

The authors gratefully acknowledge the financial support of the Kempe Foundation (Kempestiftelserna) (https://www.kempe.com/) for grant number JCSMK22-0144, which made this research possible. We also extend our sincere gratitude to **Professor Florian Schmidt** from Umeå University for providing the essential equipment that significantly contributed to our study.

Data availability

Data will be made available on request.

References

[1] K. Harding, Handbook of Optical Dimensional Metrology, CRC Press, 2013.
[2] S. Zhang, Handbook of 3D machine vision: Optical metrology and imaging, CRC Press, 2013.
[3] D. Khodadad, et al., Temperature sensing in space and transparent media: advancements in off-Axis digital holography and the temperature coefficient of refractive index, Appl. Sci. 13 (14) (2023) 8423.
[4] C.A. Barrios, Highly sensitive refractometric sensing system based on the combination of lensing and laser speckle correlation, Opt. Lasers Eng. 177 (2024) 108122.
[5] H.M. Park, et al., Polarization-multiplexed snapshot lateral shearing interferometric sensor for surface roughness measurements, Opt. Lasers Eng. 179 (2024) 108272.
[6] K. Kalita, P.K. Boruah, U. Sarma, Studies on change of strain developed in different wood samples due to change in relative humidity, Sens. Bio-Sens. Res. 22 (2019) 100264.
[7] R.S. Sirohi, Speckle Metrology, CRC Press, 2020.
[8] D. Khodadad, et al., Full-field 3D deformation measurement: comparison between speckle phase and displacement evaluation, Appl. Opt. 55 (27) (2016) 7735–7743.
[9] D. Khodadad, E. Hällstig, M. Sjödahl, Dual-wavelength digital holographic shape measurement using speckle movements and phase gradients, Opt. Eng. 52 (10) (2013) 101912.
[10] D. Khodadad, E. Hällstig, M. Sjödahl, Shape reconstruction using dual wavelength digital holography and speckle movements, Proc.SPIE 8788 Optical Measurement Systems for Industrial Inspection VIII, (2013) 87880I, https://doi.org/10.1117/12.2020471.
[11] T. Li, et al., Single-shot absolute 3D measurement based on speckle-embedded fringe projection, Opt. Lasers Eng. 172 (2024) 107884.
[12] G.H. Kaufmann, Advances in Speckle Metrology and Related Techniques, John Wiley & Sons, 2011.
[13] R. Jamali, et al., Surface characterization of biodegradable nanocomposites by dynamic speckle analysis, Appl. Surface Sci. Adv. 16 (2023) 100429.
[14] A. Mujeeb, V. Nayar, V. Ravindran, Electronic speckle pattern interferometry techniques for non-destructive evaluation: a review, Insight-Non-Destructive Test. Condition Monitoring 48 (5) (2006) 275–281.
[15] P. Bergström, et al., Dual-wavelength digital holography: single-shot shape evaluation using speckle displacements and regularization, Appl. Opt. 53 (1) (2014) 123–131.
[16] J.M. Ali, H.S. Jailani, M. Murugan, Surface roughness evaluation of electrical discharge machined surfaces using wavelet transform of speckle line images, Measurement 149 (2020) 107029.
[17] J. Heikkinen, G.S. Schajer, Self-calibrated defocused speckle imaging for remote surface motion measurements, Opt. Lasers Eng. 173 (2024) 107914.
[18] C. Xiong, et al., Specular surface deformation measurement based on projected-speckle deflectometry with digital image correlation, Opt. Lasers Eng. 170 (2023) 107776.
[19] D. Khodadad, Combined reduced phase dual-directional illumination digital holography and speckle displacements for shape measurement, Int. J. Opt. 2019 (2019) 4906109.
[20] M. Sjödahl, E. Hallstig, D. Khodadad, Multi-spectral speckles: Theory and applications, in: SPECKLE 2012: V International Conference on Speckle Metrology, SPIE, 2012.
[21] M. Sjödahl, Some recent advances in electronic speckle photography, Opt. Lasers Eng. 29 (2–3) (1998) 125–144.
[22] T. Fricke-Begemann, Three-dimensional deformation field measurement with digital speckle correlation, Appl. Opt. 42 (34) (2003) 6783–6796.
[23] K. Basak, M. Manjunatha, P.K. Dutta, Review of laser speckle-based analysis in medical imaging, Med. Biol. Eng. Comput. 50 (2012) 547–558.
[24] C. Abou Nader, et al., A new insight into biospeckle activity in apple tissues, Sensors 19 (3) (2019) 497.

[25] Y. Dong, B. Pan, A review of speckle pattern fabrication and assessment for digital image correlation, Exp. Mech. 57 (2017) 1161–1181.
[26] S.S. Beauchemin, J.L. Barron, The computation of optical flow, ACM Comput. Surveys (CSUR) 27 (3) (1995) 433–466.
[27] I. Misra, et al., Feature based remote sensing image registration techniques: a comprehensive and comparative review, Int. J. Remote Sens. 43 (12) (2022) 4477–4516.
[28] A.A. Goshtasby, Image Registration: Principles, Tools and Methods, Springer Science & Business Media, 2012.
[29] F. Jurie, M. Dhome, A simple and efficient template matching algorithm. in Proceedings Eighth IEEE International Conference on Computer Vision, in: ICCV 2001, IEEE, 2001.
[30] B. Pan, Digital image correlation for surface deformation measurement: historical developments, recent advances and future goals, Meas. Sci. Technol. 29 (8) (2018) 082001.
[31] B. Chen, S. Coppieters, Unified digital image correlation under meshfree framework, Strain 60 (1) (2024) e12461.
[32] T. Chu, W. Ranson, M.A. Sutton, Applications of digital-image-correlation techniques to experimental mechanics, Exp. Mech. 25 (1985) 232–244.
[33] Y. Lu, W. Zhu, Convolution finite element based digital image correlation for displacement and strain measurements, Comput. Methods Appl. Mech. Eng. 419 (2024) 116597.
[34] W. Peters, W. Ranson, Digital imaging techniques in experimental stress analysis, Opt. Eng. 21 (3) (1982) 427–431.
[35] G. Besnard, F. Hild, S. Roux, "Finite-element" displacement fields analysis from digital images: application to Portevin–Le Châtelier bands, Exp. Mech. 46 (2006) 789–803.
[36] X. Tong, et al., Image registration with Fourier-based image correlation: a comprehensive review of developments and applications, IEEE J. Selected Top. Appl. Earth Observ. Remote Sens. 12 (10) (2019) 4062–4081.
[37] C.D. Kuglin, The Phase Correlation Image Alignment Method, 1975.
[38] F.R. Hampel, Contributions to the Theory of Robust Estimation, University of California, Berkeley, 1968.
[39] F.R. Hampel, et al., Robust Statistics, Wiley Series in Probability and Statistics, 2005.
[40] D. Khodadad, et al., Single shot dual-wavelength digital holography: calibration based on speckle displacements, Int. J. Optomechatron. 8 (4) (2014) 326–339.
[41] F.J. Harris, On the use of windows for harmonic analysis with the discrete Fourier transform, Proc. IEEE 66 (1) (1978) 51–83.
[42] D. Khodadad, Multiplexed Digital Holography Incorporating Speckle Correlation, Luleå tekniska universitet, 2016.
[43] P. Zhou, K.E. Goodson, Subpixel displacement and deformation gradient measurement using digital image/speckle correlation (DISC), Opt. Eng. 40 (8) (2001) 1613–1620.
[44] R. Xue, et al., Applying machine learning to optical metrology: a review, Meas. Sci. Technol. 36 (1) (2025) 012002.
[45] X. Hao, et al., A quantitative laser speckle-based velocity prediction approach using machine learning, Opt. Lasers Eng. 166 (2023) 107587.